NEUTRINO OSCILLATIONS AT ACCELERATORS

MAURO MEZZETTO
Istituto Nazionale di Fisica Nucleare and Dept. of Physics "G. Galilei", Via Marzolo 8, 35131 Padova, Italy
E-mail: mezzetto@pd.infn.it

1. Introduction

Neutrino oscillations were firstly suggested by B. Pontecorvo [1] in the late fifties. It took about twenty years to have the first experimental results from reactors [2] and from accelerators [3]. The present generation of neutrino oscillation experiments, 20 more years later, is mature enough to produce firm and serious claims of signal.

The clear advantage of neutrino beams from accelerators derives from the possibility to generate intense fluxes with a good control of the production processes; they are the only source of neutrinos where appearance experiments can be performed. The major drawback is the difficulty to explore the regions of very low Δm^2 (below $10^{-3} eV^2$) given the unlikely possibility to use very long baselines.

The present generation of accelerator experiments searches for $\overline{\nu}_\mu \rightarrow \overline{\nu}_e$ oscillations using ν beams produced at low energy proton beam dump and for ν_τ appearance in a ν_μ beams produced by a high energy proton.

The experiments are probing the Δm^2 region relevant to neutrinos masses of cosmological interest: $0.5 < \Delta m^2 < 50\ eV^2$.

2. $\overline{\nu}_\mu \rightarrow \overline{\nu}_e$ experiments at beam dump

Two experiments are looking for $\overline{\nu}_\mu \rightarrow \overline{\nu}_e$ oscillations at beam dump.

The LSND experiment runs at the Los Alamos Meson Physics Facility (LAMPF), while the KARMEN experiment runs at the ISIS neutron spallation facility at the Rutherford-Appleton laboratory. Both use a 800 MeV kinetic energy proton beam hitting a target located next to a beam dump. The basic concepts of these experiments were outlined by B. Pontecorvo already in 1960 [4].

Most of the produced π^+ come to rest (decay at rest: DAR) in the dump producing the decay chain $\pi^+ \rightarrow \mu^+ \nu_\mu$ followed by $\mu^+ \rightarrow \overline{\nu}_\mu\, e^+ \nu_e$ (fig. 1). On the contrary most of the π^- ($\sim 1/8$ of the π^+) are absorbed by the high Z dump material and eventually their μ^- daughters are captured. So the $\overline{\nu}_e$ flux, coming from μ^- decay in flight (DIF), is highly suppressed (fig. 1): in LSND $\overline{\nu}_e / \overline{\nu}_\mu$ is $0.78 \cdot 10^{-3}$ [5]. These experiments are able to explore $\overline{\nu}_\mu \rightarrow \overline{\nu}_e$ oscillation for probabilities of the order of 10^{-3}.

Both the experiments can not distinguish e^+ from e^-, but the $\overline{\nu}_e$ interactions are tagged through the process:

$$\overline{\nu}_e\, p \rightarrow e^+ n \qquad E_e < 52.8\, MeV \tag{1}$$

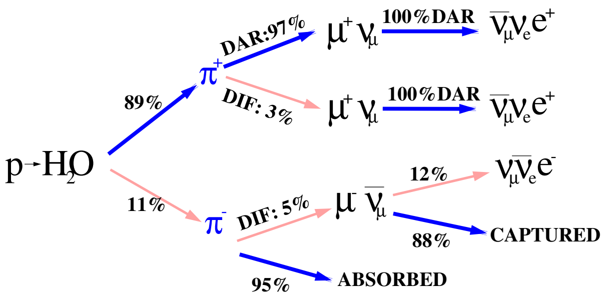

Fig. 1. Sketch of the ν production chain in LSND (water target).

thanks to the neutron detection, while ν_e interact mainly through the reaction

$$\nu_e \ {}^{12}C \rightarrow e^- \ {}^{12}N \qquad E_e < 36MeV \tag{2}$$

and the only reaction producing both an electron and a neutron is

$$\nu_e \ {}^{12}C \rightarrow e^- n \ {}^{12}N \qquad E_e < 20MeV \tag{3}$$

Therefore no background can be generated by ν_e interactions with electrons above $20MeV$.

The KARMEN experiment can furthermore exploit the time structure of the ISIS proton beam, separating in time neutrinos coming from μ^+ DAR from those resulting from π decay.

2.1. LSND experiment

LSND uses a single tank of diluted scintillator, 8.75 m long, at a mean distance of 30 m (17^0) from the target fig. 2 [5]. Both $\hat{C}$erenkov and scintillation light are detected by an array of 1220 8" PMTs (25% of surface coverage).

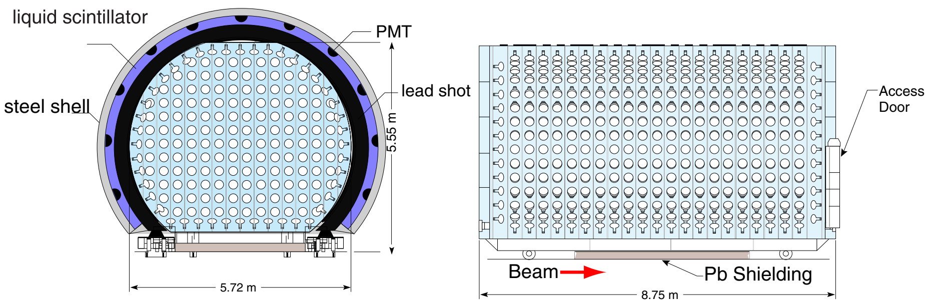

Fig. 2. Front and side view of the LSND detector.

The main analysis steps are:

1. Particle identification through position, direction, number of hit PMTs. The positron identification is enhanced by the possibility of discriminate $\hat{C}$erenkov from scintillation light. The electron calibration can be performed measuring e^- generated by the decay of μ from cosmic rays.

2. Cosmic rays are discriminated by a veto on detector activity before and after the trigger.

3. Neutrons are detected by observing the 2.2 MeV γ ray from the process p(n,γ)D in the scintillator. A likelihood function R is built to separate e^+n correlated events from backgrounds, using the time information, the spatial information and the number of hit PMTs.

4. Positron energy range: $20 \leq E_e \leq 60\ MeV$.

The overall $\overline{\nu}_e$ detection efficiency is $\sim 22\%$

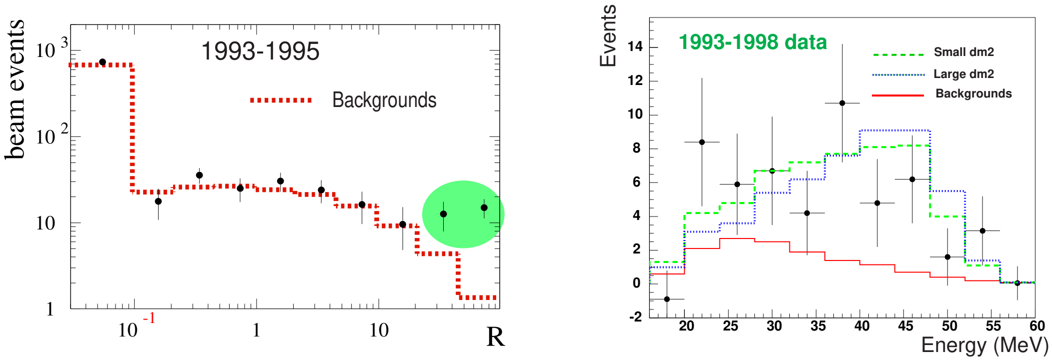

Fig. 3. Left: (a) distribution of the likelihood function R, used to identify correlated e^+n events, compared with the background predictions. This plot contains events of the 1993-95 runs, corresponding to about half the final statistic of the experiment. Right: (b) energy distribution of the candidate events compared with the expectations for oscillations at large ($>> 1eV^2$) δm^2 (dotted), small δm^2 (dashed) and background predictions (solid line).

The excess of e^+n events is well visible from the R distribution of the candidate events compared with the predictions, fig. 3a). The energy distribution of the excess events is in agreement with what expected from neutrino oscillation, fig. 3b).

70 candidate events with $R > 30$ have been collected in the 1993-1998 data taking period (total charge on target 28743 C) to be compared with the expectations of 17.7 ± 1.1 beam off events, 7.9 ± 1.4 events from neutrino interactions randomly correlated with a neutron and 4.9 ± 0.9 from neutrino interactions correlated with a neutron; these are the only background events estimated through a MC calculation, while the others are directly measured in the experiment; there are $\overline{\nu}_e\ p \rightarrow e^+n \quad (3.3 \pm 0.7)$, $\overline{\nu}_\mu\ p \rightarrow \mu^+n \quad$ from$\pi^-\overline{\nu}_\mu\ DIF \quad (1.5 \pm 0.6)$ and $\overline{\nu}_e\ p \rightarrow e^+n \quad (0.1 \pm 0.1)$. In order to explain the event excess the MC predictions should be wrong by more than a factor 8. This excess of 39.5 ± 8.8 events corresponds to a $\overline{\nu}_\mu \rightarrow \overline{\nu}_e$ oscillation probability[6)]

Year	Coulomb	Beam ON	Beam Off	ν bgd	Excess	Oscill. Prob.(%)
93-95	14772	38	9.2 ± 0.8	7.7 ± 0.8	21.1 ± 6.3	$0.31 \pm 0.12 \pm 0.05$
96-98	13971	32	8.5 ± 0.6	5.1 ± 0.6	18.4 ± 6.1	$0.32 \pm 0.15 \pm 0.05$
Total	28743	70	17.7 ± 1.0	12.8 ± 1.7	39.5 ± 8.8	$0.31 \pm 0.09 \pm 0.05$

Table 1. Candidate events in LSND with $R > 30$ and $20 < E_e < 60$.

$$P(\overline{\nu}_\mu \rightarrow \overline{\nu}_e) = [3.1 \pm 0.9(stat.) \pm 0.5(syst.)] \cdot 10^{-3} \tag{4}$$

The signal region in the $(sin^2(2\theta), \Delta m^2)$ plane, fig. 4, is built using 4 variables: the energy, the likelihood function R, the angle with the beam direction and the path length of all the events with $R > 0$. The signal region is defined by a bidimensional grid selecting $\Delta\chi^2 \leq 2.6$ (90 %) and $\Delta\chi^2 \leq 4.5$(99%) above the minimum.

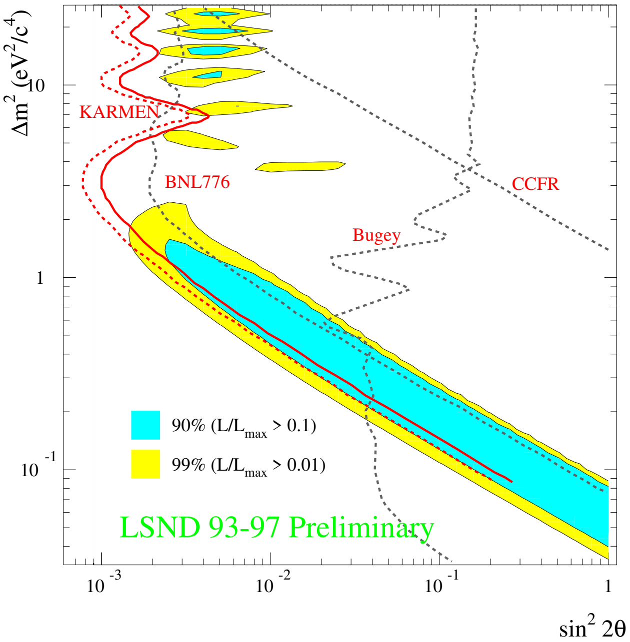

Fig. 4. Preliminary plot of the preferred signal region of LSND (1993-97) compared with the preliminary feb97-nov98 90%CL limit of KARMEN (solid line). Also shown are the expected sensitivity of KARMEN at the end of the data taking (dashed line) and the limits of previous experiments at accelerators (CCFR, ref. [10]) and BNL776, ref. [11]) and at reactors (Bugey, ref. [12])).

The LSND collaboration has also reported an independent evidence for the oscillation signal from the observation of an excess of beam associated electrons in the energy range $60 < E_e < 200$ MeV as expected from the inclusive reaction $\nu_e + C^{12} \rightarrow e^- + X$ induced by ν_μ from π^+ DIF [7]). No correlated neutron can be used to tag these events, however ν_e events from $\nu^+ \rightarrow \mu^+ - DAR$ are suppressed because they can only produce electrons with a maximum energy of 54 MeV. Furthermore in this energy range

e^- are better separated from μ^- thanks to the more favorable $\hat{C}$erenkov/scintillation light ratio. In the years 1993-1995 (14772 C) 40 e^- events have been detected while the expected background was of 10.5 ± 0.8 from beam off events and 9.6 ± 1.9 from machine related sources, giving an excess of 18.6 ± 6.6 events, corresponding to [7)]

$$P(\nu_\mu \rightarrow \nu_e) = [2.6 \pm 1.3(stat.) \pm 0.5(syst.)] \cdot 10^{-3} \tag{5}$$

The significance of this signal is less stringent than the one in the $\overline{\nu}_\mu - \overline{\nu}_e$ channel but it provides an independent confirmation from a channel with different background sources, different systematic errors and biases.

The experiment completed the data taking on December 21,1998 and a global analysis of all the data (DAR and DIF) is expected in the coming months.

2.2. KARMEN experiment

The KARMEN detector, fig. 5, is a 56 t segmented liquid scintillator calorimeter located at a mean distance of 17.5 (90^0) from the ISIS ν source. The detector is segmented in 512 independent modules, monitored by 2 PMTs at each side. Gadolinium (Gd_2O_3) deposited on thin sheets of paper and embedded in the walls of the modules allows neutron detection through Gd(n,γ) capture reaction.

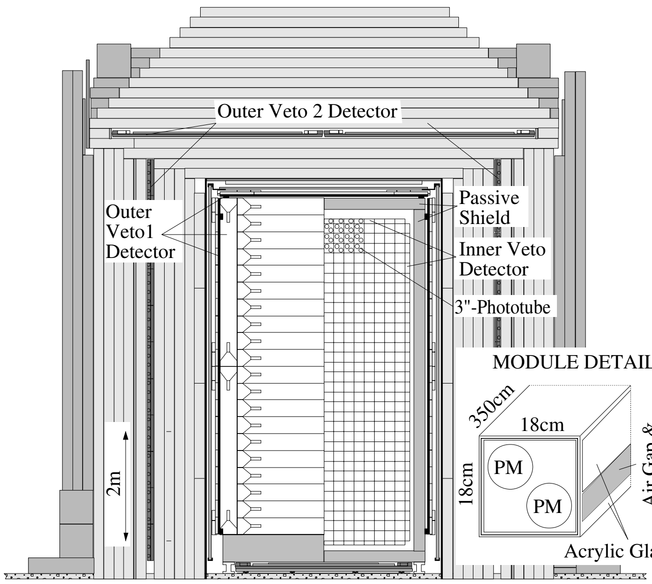

Fig. 5. The KARMEN calorimeter in the 7000 t shielding blockhouse.

The first runs of KARMEN, 1990-1995, suffered from cosmic rays background, that limited the sensitivity of the experiment. After 1995 the detector system has been upgraded with an additional veto layer embedded in the walls and the roof of the shielding blockhouse. It makes it possible to tag the cosmic muons which generate the neutrons in deep inelastic reactions in the steel veto, and consequently to reduce the cosmic background by a factor 42.

The data analysis is similar to the one of LSND: e^+n correlated events are selected by using likelihood functions and cuts are applied against the detector activity before and after the event, in order to further reject cosmics.

The data taking of the upgraded detector began in February 1997. Preliminary results from the data collected up November 1998 (3731 C) show 7 events selected against a predicted background of 9.30 ± 0.74 events, so that $P(\overline{\nu}_\mu \rightarrow \overline{\nu}_e) \leq 3.8 \cdot 10^{-3}\,(90\%CL)$, [8]. The corresponding exclusion plot, built with the unified approach method [9], is shown in fig. 4 compared with the signal plot of LSND. The experiment will run until 2001, its final sensitivity[a] is expected to be $P(\overline{\nu}_\mu \rightarrow \overline{\nu}_e) \leq 2.6 \cdot 10^{-3}\,(90\%CL)$, so that a negative result from KARMEN will not be enough to rule out the LSND signal (see also fig. 4).

	LSND	KARMEN
Accelerator	LAMPF	ISIS
Proton Energy	800 MeV	800 MeV
Proton Current	1 mA	0.2 mA
Duty factor	$6 \cdot 10^{-2}$	$5 \cdot 10^{-4}$
Angle from proton beam axis	17^0	90^0
Distance from target	30 m	17.5 m
Timing separation μ/π	No	Yes
Detector mass	167 tons	56 tons
Detection	Scint + Čerenkov	Scint.
Event location	timing	segmentation
Energy resolution	$\frac{43\%}{\sqrt{E\,(MeV)}}$	$\frac{11\%}{\sqrt{E\,(MeV)}}$
Particle id.	Yes	No
Neutron capture	proton (2.2 $MeV\gamma$)	Gd (8 $MeV\ \gamma$)
Integrated charge	$\sim 28700\ C$	9211+3731 C
Relative Detection Event Rate ($\overline{\nu}_e + p \rightarrow e^+ + n$)		
High $\Delta m^2 (> 10\,eV^2)$	1.0	0.24
Small $\Delta m^2 (< 1\,eV^2)$	1.0	0.08

Table 2. Comparison of LSND and KARMEN experiments. For a detailed comparison of the two experiments see also ref. [13]

[a]Sensitivity is defined as the average limit for an experiment that doesn't see any signal and detects the expected background.

3. $\nu_\mu \to \nu_\tau$ oscillation at CERN WANF

Two experiments, NOMAD and CHORUS, took data between 1994 and 1998 at the CERN wide band neutrino beam from the 450 GeV CERN proton synchrotron (SPS). The beam consists primarily of ν_μ , with a small contamination of ν_e ($\sim 1\%$), while the ν_τ contamination is negligible (fig. 3). The average distance between the ν_μ source and the detector was $\sim 630\,m$.

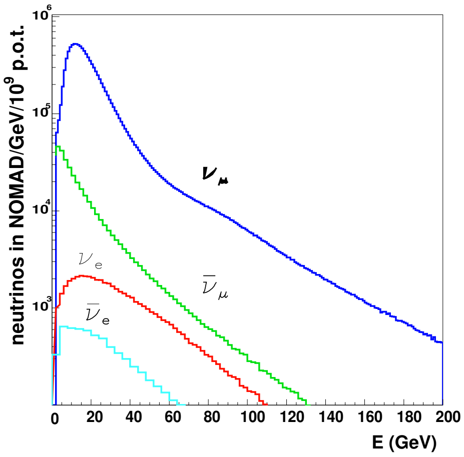

Flavor	Rel. Flux	$\langle E_\nu \rangle$ (GeV)
ν_μ	1	23.5
$\overline{\nu}_\mu$	0.061	19.2
ν_e	0.0094	37.1
$\overline{\nu}_e$	0.0024	31.3
ν_τ	$\simeq 5 \cdot 10^{-6}$	35

Table 3. Mean energy and relative abundances for ν fluxes in the NOMAD fiducial volume.

The two experiments were the first round of dedicated searches of $\nu_\mu \to \nu_\tau$ oscillations at accelerators.

CHORUS and NOMAD followed two complementary methods to identify ν_τ charged current (CC) interactions sketched in fig. 6. The former based its search on the detection of the decay particle from the short lived τ^- in the one prong configuration (kink), while the latter used the measured kinematical characteristics of the tau decay in the transverse plane, as firstly suggested in ref. [14].

3.1. CHORUS

At the energies of the WANF beam the τ path length is $c\gamma\tau \simeq 1mm$. The only detector with the needed resolution is nuclear emulsion, (spatial resolution $\sim 1\mu m$, grain density: $\sim 300/mm$) the experiment used emulsions of an unprecedent mass: 770 kg. To predict the track position in the emulsion bulk special emulsion sheets followed by scintillating fibers [17] (2 mrad and 150 μm resolution) were used. The target region was followed by an air-core hexagonal magnet, high resolution

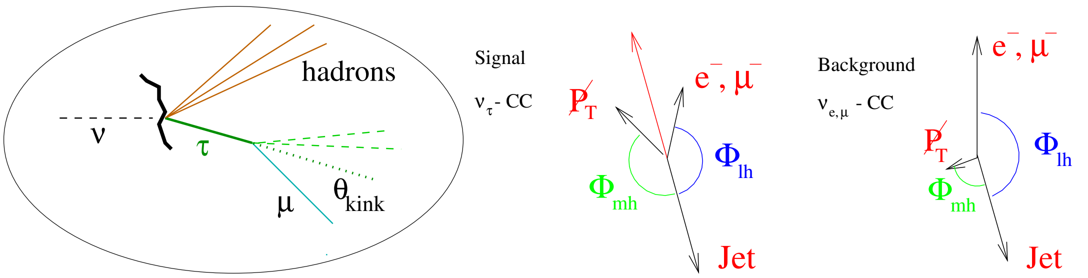

Fig. 6. Sketch of the detection procedures of τ decays in CHORUS, left, and NOMAD, right. In CHORUS the τ track is identified by it characteristic path length and the angle respect its charged daughter. In NOMAD the principal signature for the leptonic τ decays are the transverse plane angles Φ_{mh} and Φ_{eh} between the momentum of the hadron jet p^T_{had} , and the missing momentum p^T_{miss} or the lepton daughter p^T_{lep} . While in the signal p^T_{miss} and p^T_{lep} are correlated (the τ decaying in a lepton and two neutrinos), in the charged current background events little room is left to the p^T_{miss} and its direction is randomly distributed.

electromagnetic and hadron calorimeters and a muon spectrometer, fig. 7 [16].

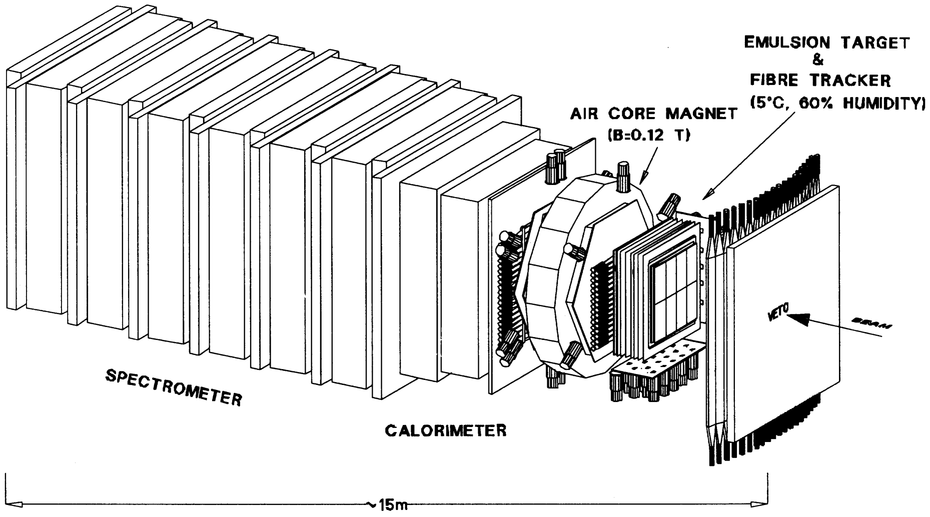

Fig. 7. Side view of the CHORUS detector.

In the analysis the emulsion scanning procedure to locate the interaction point and to reject events incompatible with τ decays is fully automatic. The remaining events undergo a computer assisted eye scan to confirm the presence of a τ decay. Events with 2 muons in the final state ($\sim 2\%$ of the total) are selected to check the scanning efficiency, searching for a kink in a muon track (D^+ decay): the results are summarized in tab.4

A key factor of the experiment is the dramatic increase of the microscope scanning speed: a factor 360 from 1994 to 1998, moreover and additional factor 10 is expected for the year 2000. This increase of scanning speed allows to use less stringent criteria

	1995	1996
Expected events	7.4 ± 0.7	15.4 ± 2.2
Events found	8	17

Table 4. Predictions and results on the search for dimuon events with a visible kink in CHORUS.

to select the events to be measured, gaining in efficiency and reducing the biases [15].

The τ search looks for events with 1 or 0 negative muons in the final state which show a kink near the origin. The first case, sensitive to the $\tau \to \mu^- \overline{\nu}_\mu \, \nu_\tau$ decay channel, is nearly background free since the background can only come from charm production by $\overline{\nu}_\mu$ interactions, when the leading μ is not identified and turns out to be negligible. This analysis [18] looks for a negative μ track with a momentum $p < 30 \, GeV/c$, no other primary lepton, a kink on muon track with a $p_\top > 250 \, MeV/c$, and a short flight length of the parent track less than 5 emulsion plates, corresponding to 4 mm.

The other channel looks for 0μ events and is sensitive to three decay modes of the tau: $\tau \to 1h^- + X$, $\tau \to e^- \overline{\nu}_e \, \nu_\tau$ (and $\tau \to \mu \, \overline{\nu}_\mu \, \nu_\tau$ when the μ was not identified). This analysis [19] looks for a negative non-muon track with a momentum $1 < p < 20 \, GeV/c$, no primary lepton, a kink on negative track $p_\top > 250 \, MeV/c$ and a strict cut on the τ candidate flight length, less than 3 emulsion plates. In this channel the main source of background are neutral current (NC) events with a "white kink": namely a hadronic interaction where a hadron has a 1-prong nuclear interaction without other ionizing tracks and no evidence for nuclear break up. This background is estimated to be of 0.5 events with the present statistic; it is evaluated thanks to the results of a dedicated experiment [20], but it will be better measured in CHORUS by scanning pion tracks in the emulsions far from the primary vertex, searching for the white kink frequency.

No candidate events have been found analyzing about 50% of the 1μ events and 20% of the 0μ events. After taking into account the decay branching ratio and detection efficiencies, table 5, this negative result provides the limit on $\nu_\mu \to \nu_\tau$ oscillations

	1μ	$0\mu(h)$	$0\mu(e^-)$	$0\mu(\not{\mu})$
$A(\tau)$	0.39	0.17	0.093	0.026
B.R.	0.174	0.495	0.178	0.174
ϵ	0.35-0.52	0.26	0.13	0.25
$N_\tau^{\max}$	4003	998	100	51

Table 5. Summary of the efficiencies of the CHORUS analysis. $N_\tau^{\max}$ is the maximum number of expected signal events for full mixing. About 50% of the final statistic has been analyzed, in the 1μ channel and about 20% for the 0μ one.

$$P(\,\nu_\mu \to \nu_\tau\,) \leq 4.6 \cdot 10^{-4} \quad (90\% CL), \tag{6}$$

the corresponding exclusion plot is shown in fig. 10.

3.2. NOMAD

The NOMAD experiment combines the spectrometric capabilities of bubble chambers with the hermeticity granted by a high resolution electromagnetic calorimeter and large area muon chambers.

The NOMAD detector, fig. 8, is described in ref. [21]. Inside a 0.4 T magnetic field, it consisted of an active target (2.7 tons) made of drift chambers followed by a transition radiation detector [22], a preshower detector, and an electromagnetic calorimeter [23]. A hadron calorimeter and two muon identification stations were located just after the magnet coil. The neutrino interaction trigger [24] consisted of a coincidence between two planes of counters located after the active target, in the absence of a signal from a large area system of veto counters in front of the NOMAD detector.

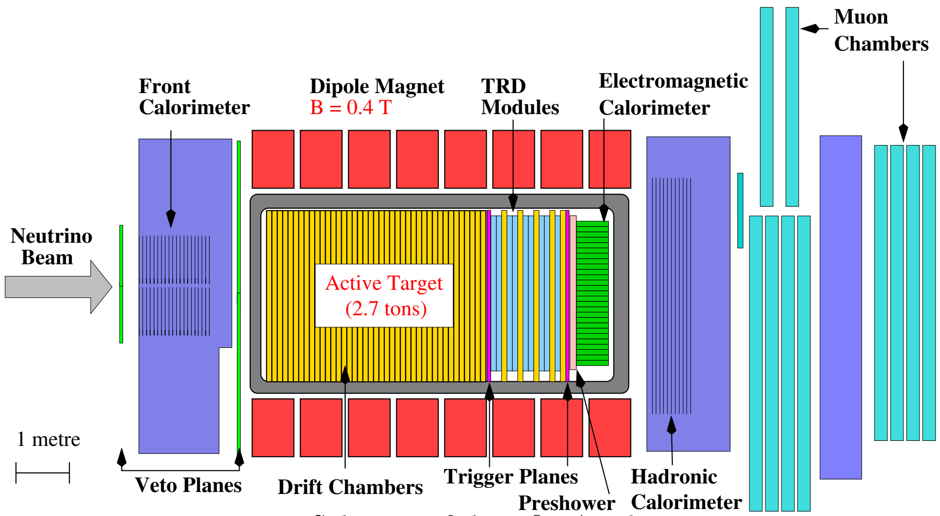

Fig. 8. Side view of the NOMAD detector

The analysis steps are:

1. Quality cuts based on approximate charge balance at the primary vertex and on the estimated momentum and energy errors; they typically remove 15% of the events.

2. Identification of the particle (or particles) consistent with being produced in τ decay.

3. Reconstruction of the associated hadronic system,

4. Use of kinematic variables to separate the signal from background.

Unfortunately no single variable unambiguously identifies a τ, but the distributions of several kinematical variables - like the missing momentum p^T_{miss}, the Φ_{eh} and Φ_{mh} angles in the transverse plane (fig.6), the momentum of the τ charged daughter respect the hadron beam (q_t) that discriminates signal from NC backgrounds - are different for the τ signal and the various backgrounds. Therefore, the information is optimized by combining these variables into a likelihood ratio function.

Separate analysis procedure have been developed for ν_τ CC interactions with deep-inelastic scattering (DIS) configurations or with quasi elastic like configurations (LM), the two are distinguished by requiring that total hadron momentum p_{had} be above or below 1.5 GeV/c.

In order to reliably compute background rejection factors as large as 10^5, the MC results are implemented using a "data simulator" method based on the data themselves. In a sample of measured ν_μ CC events the identified muon is replaced with a MC-generated lepton (DS events), so that fake NC, $\nu_e CC$ or τ events can be generated. The same procedure can be applied to reconstructed ν_μ CC MC events (MCS events). All signal and background efficiencies ϵ are then obtained from the relation $\epsilon = \epsilon_{\rm MC} \times \epsilon_{\rm DS}/\epsilon_{\rm MCS}$.[b] The DS correction ranges from 1.2 to 1.8 in the different channels. After the correction the agreement between MC predictions and the data is quite good, as can be seen in fig. 9 and table 6.

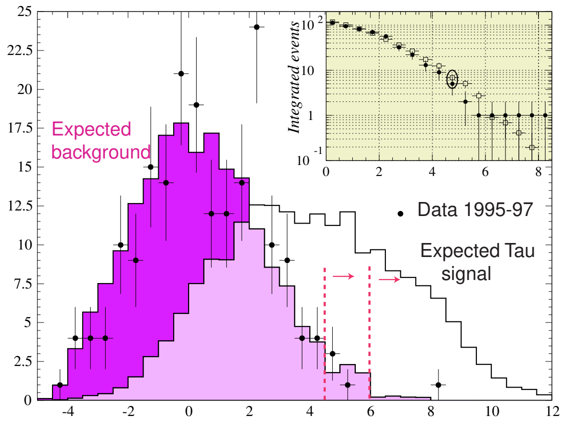

Fig. 9. Histogram of the final likelihood function for the events selected by the $\tau \to e\nu_\tau \overline{\nu}_e$ DIS NOMAD analysis (dots). Also shown are the expectations for the sum of backgrounds (shaded) and the expected signal. The inset gives the integral likelihood distribution for the data (dots) and expected backgrounds (squares); the encircled points are at the boundary of the signal region.

A "blind analysis" technique is used to avoid biases that can be introduced if the data are examined in the "signal region" before the analysis is demonstrated to be

[b]Following this prescription the decay channel $\tau \to \mu\overline{\nu}_\mu \nu_\tau$, that potentially could contribute for a 10% of the final sensitivity, cannot be used, since it cannot be corrected with the data simulator method.

robust. A "box" is defined around the region where the signal to background ratio is expected to be higher (signal region). The data cannot be analyzed inside the box until the analysis procedure can predict and check the background outside the box, as well as in the τ^+ searches (given the beam composition no τ^+ signal is expected).

In table 6 are summarized the results of the analyses in the various τ decay channels, DIS searches have already analyzed about 70% of collected data, LM searches about 15%.

		τ^-		τ^+				
Analysis	Year	Obs.	Est. Bkgnd	Obs.	Est. Bkgnd	$\epsilon(\%)$	$Br(\%)$	$N_\tau^{\max}$
$\tau \to e$ DIS	95-97	5	$6.3^{+1.6}_{-1.0}$	7	7.4 ± 3.1	3.5	17.8	2818
$\tau \to h(n\pi^0)$ DIS	95-97	5	5.0 ± 1.2	14	9.9 ± 2.3	0.78	49.8	1727
$\tau \to \rho$ DIS	95-97	5	$5.0^{+1.7}_{-0.9}$	13	$10.2^{+1.4}_{-1.1}$	1.6	25.3	1891
$\tau \to 3\pi(\pi^0)$ DIS	95-96	5	6.5 ± 1.1	14	13.5 ± 1.4	2.9	15.2	1180
$\tau \to e$ LM	95	0	$0.5^{+0.6}_{-0.2}$	1	1.1 ± 0.7	3.4	17.8	218
$\tau \to \pi(\pi^0)$ LM	95	1	$0.1^{+0.3}_{-0.1}$	6	8.8 ± 3.5	1.5	37.3	198
$\tau \to 3\pi(\pi^0)$ LM	95	0	$0.4^{+0.6}_{-0.4}$	14	11 ± 4	2.0	15.2	108

Table 6. Summary of backgrounds and efficiencies for the NOMAD analysis for negative and positive candidates. 1995-97 data correspond to 950000 ν_μ CC interactions in the target, 1995 data to 140000 ν_μ CC interactions.

The resulting 90% CL upper limit on the oscillation probability is

$$P(\nu_\mu \to \nu_\tau) < 6 \cdot 10^{-4} \quad (90\% \, CL) \tag{7}$$

The exclusion in the $(\Delta m^2,\ sin^2(2\theta))$ plane is shown in fig. 10 together with the corresponding exclusion plot of CHORUS.

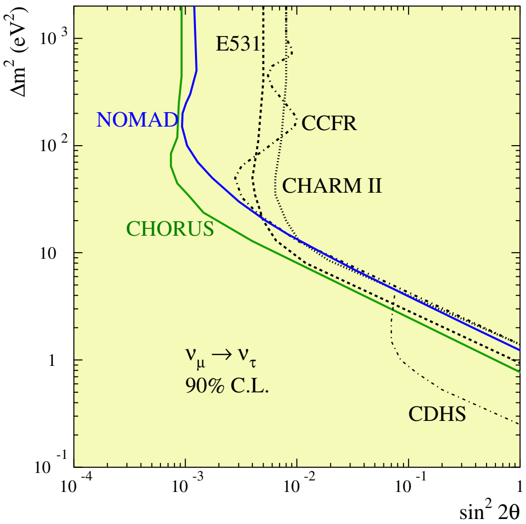

Fig. 10. Exclusion region (90% CL) for $\nu_\mu \to \nu_\tau$ oscillations from CHORUS and NOMAD together with the exclusion regions from previous experiments.

4. Acknowledgements

I am grateful to M. Baldo Ceolin, my colleagues in Padova, E. Fiorini, L. Di Lella, P. Strolin, P. Zucchelli, A. Fazely, W.C. Louis and G. Drexlin for the nice discussions and the information about their experiments.

5. References

1) B. Pontecorvo, *Zh. Eksp. Theor. Fiz.* **33**, 549 (1957), *Zh. Eksp. Theor. Fiz.* **34**, 247 (1958).
2) H.W. Sobel, F. Reines and E. Pasierb, Neutrino Physics and Astrophysics, ed. by E. Fiorini, Plenum Press, 1980, pag. 241
3) E. Bellotti, D. Cavalli, E. Fiorini and M. Rollier, Lett. Nuovo Cim. 17 (1976) 553.
4) B. Pontecorvo, J. Exptl. Theoret. Phys. (USSR), 1959, Vol. 37, pages 1751-7. Reprinted in K. Winter, Neutrino Physics, Cambridge University Press, 1991, page 46-55.
5) C. Athanassopoulos *et al.*, Nucl. Instrum. Meth. **A388**, 149 (1997) nucl-ex/9605002.
6) C. Athanassopoulos *et al.* [LSND Collaboration], Phys. Rev. Lett. **75**, 2650 (1995). C. Athanassopoulos *et al.* [LSND Collaboration], Phys. Rev. Lett. **77**, 3082 (1996). C. Athanassopoulos *et al.* [LSND Collaboration], Phys. Rev. **C54**, 2685 (1996) D.H. White, Neutrino '98, Takayama, Japan, 4-9 june 1998. E.D. Church, DPF 99, UCLA, 5-9 january 1999.
7) C. Athanassopoulos *et al.* [LSND Collaboration], Phys. Rev. **C58**, 2489 (1998) C. Athanassopoulos *et al.* [LSND Collaboration], Phys. Rev. Lett. **81**, 1774 (1998)
8) K. Eitel *et al.* [KARMEN Collaboration], Neutrino '98 Takayama, Japan; 4 - 9 Jun 1998, hep-ex/9809007. R. Maschuw, WIN99, Cape Town, South Africa, 24-30 January 1999.
9) G.J. Feldman, R.D. Cousins, Phys. Rev. **D 57** (1998) 3873.
10) A. Romosan *et al.* [CCFR/NuTeV Collaboration], Phys. Rev. Lett. **78**, 2912 (1997)
11) L. Borodovsky *et al.* [BNL-E776 Collaboration], Phys. Rev. Lett. **68**, 274 (1992)
12) Y. Declais *et al.*, Nucl. Phys. **B434**, 503 (1995).
13) S.J. Yellin, hep-ex/9902012.
14) C.H. Albright, R.E. Shrock, Phys. Lett. **B84**, 123 (1979).
15) K. Niwa, this conference proceedings.

16) E. Eskut *et al.* [CHORUS Collaboration], Nucl. Instrum. Meth. **A401**, 7 (1997).
17) P. Annis [CHORUS Collaboration], Nucl. Instrum. Meth. **A412**, 19 (1998).
18) E. Eskut *et al.* [CHORUS Collaboration], Phys. Lett. **B434**, 205 (1998).
19) E. Eskut *et al.* [CHORUS Collaboration], Phys. Lett. **B424**, 202 (1997).
20) K. Kodama *et al.*, FERMILAB P803 Proposal (1993), Appendix D.
21) J. Altegoer *et al.* [NOMAD Collaboration], Nucl. Instrum. Meth. **A404**, 96 (1997).
22) G. Bassompierre et al., Nucl. Instr. and Meth. **A 403** (1998) 363; G. Bassompierre et al., Nucl. Instr. and Meth. **A 411** (1998) 63.
23) D. Autiero et al., Nucl. Instr. and Meth. **A 372** (1996) 556; D. Autiero et al., Nucl. Instr. and Meth. **A 373** (1996) 358; D. Autiero et al., Nucl. Instr. and Meth. **A 387** (1997) 352.
24) J. Altegoer et al., CERN-EP/98-202, accepted for publication in Nucl. Instr. and Meth. A.
25) P. Astier *et al.* [NOMAD Collaboration], Phys. Lett. **B453**, 169 (1999).